Ocean Modelling 130 (2018) 29–39

Contents lists available at ScienceDirect

Ocean Modelling

journal homepage: www.elsevier.com/locate/ocemod

The wind work input into the global ocean revealed by a 17-year global HYbrid coordinate ocean model reanalysis

Zhitao Yu[a,*], Yalin Fan[a], E. Joseph Metzger[a], Ole Martin Smedstad[b]

[a] Naval Research Laboratory, Stennis Space Center, MS, USA
[b] Vencore, Incorporated, Stennis Space Center, MS, USA

A B S T R A C T

A 17-year (1999–2015) HYbrid Coordinate Ocean Model (HYCOM) reanalysis is used to calculate the wind work to the global oceanic circulation with a focus on the global integral of the wind work on the ageostrophic currents. While the wind work on the geostrophic currents estimate of the study is in good agreement with previous research, our estimation of the wind work on the ageostrophic currents (5.44 TW) is significantly larger than previous estimates. The two main reasons for this difference are: (1) the thickness of HYCOM's first vertical layer is 1 m and thus the surface ageostrophic currents are better represented than those in numerical models that use a thicker top layer; and (2) the reanalysis is forced with hourly surface stresses and thus contains wind work contributions from high frequency wind stress variations compared against previous estimates using daily wind stress.

1. Introduction

The wind is one of several possible mechanical energy sources to drive ocean interior mixing (Munk and Wunsch, 1998) and the wind energy input to the global oceans is the most important mechanical energy source in maintaining the oceanic general circulation (Huang et al., 2006). The average wind mechanical energy input rate is defined as the total wind work

$$W = \overline{\boldsymbol{\tau}\cdot\boldsymbol{V}}, \tag{1}$$

where W is the rate at which the wind stress ($\boldsymbol{\tau}$) works on the ocean surface current ($\boldsymbol{V}$) and an overbar denotes time averaging.

The ocean surface current in Eq. (1) can be split into geostrophic ($\boldsymbol{V_g}$) and ageostrophic ($\boldsymbol{V_{ag}}$) components:

$$\boldsymbol{V} = \boldsymbol{V_g} + \boldsymbol{V_{ag}}. \tag{2}$$

Thus, the wind work input into the global ocean circulation contains both wind work on surface geostrophic currents (W_g) and ageostrophic currents (W_{ag}):

$$W = W_g + W_{ag} = \overline{\boldsymbol{\tau}\cdot\boldsymbol{V_g}} + \overline{\boldsymbol{\tau}\cdot\boldsymbol{V_{ag}}}. \tag{3}$$

W_g and W_{ag} can be further divided into mean and eddy parts as respectively shown in Eqs. (4) and (5):

$$W_g = \overline{\boldsymbol{\tau}}\cdot\overline{\boldsymbol{V_g}} + \overline{\boldsymbol{\tau}'\cdot\boldsymbol{V_g}'}, \tag{4}$$

$$W_{ag} = \overline{\boldsymbol{\tau}}\cdot\overline{\boldsymbol{V_{ag}}} + \overline{\boldsymbol{\tau}'\cdot\boldsymbol{V_{ag}}'}, \tag{5}$$

where the prime denotes fluctuations relative to the corresponding time average. The different components of wind work have been explored by researchers using different methodologies and demonstrated consistencies in some and disagreements in others (Wunsch, 1998; Wang and Huang, 2004; Huang et al., 2006; Von Storch et al., 2007; Hughes and Wilson, 2008).

1.1. Previous estimates of wind work on surface geostrophic currents

Many efforts have been conducted to estimate the global W_g. Prior to the satellite era, only rough estimates were possible using ship drift observations to approximate $\boldsymbol{V_g}$ and wind climatologies to estimate $\boldsymbol{\tau}$ (Fofonoff 1981; Oort et al., 1994). Wunsch (1998) provided the first detailed estimate of global W_g in the satellite era. Using geostrophic currents calculated from satellite altimetry and the National Centers for Environmental Prediction (NCEP) wind stress, he calculated a 4-year (1992–1996) average total global integral W_g as 0.88 TW (Table 1), about one half the estimate given by Fofonoff (1981) and Oorr et al. (1994). From this total, 0.84 TW comes from the mean part ($\overline{\boldsymbol{\tau}}\cdot\overline{\boldsymbol{V_g}}$) and 0.04 TW from the eddy part ($\overline{\boldsymbol{\tau}'\cdot\boldsymbol{V_g}'}$). In his calculation, both geostrophic currents and wind stresses were averaged over a 10-day period that was determined by the TOPEX/POSEIDON data, and the wind work on the geostrophic currents by higher frequency wind fluctuations was assumed to be small. Subsequently, using the TOPEX/POSEIDON data but with two different wind stress products from NCEP-National Center for Atmospheric Research (NCAR) Reanalysis I and the European Centre for Medium-Range Weather Forecasts ERA-40

* Corresponding author.
E-mail address: zhitao.yu@nrlssc.navy.mil (Z. Yu).

https://doi.org/10.1016/j.ocemod.2018.07.009
Received 23 October 2017; Received in revised form 23 July 2018; Accepted 25 July 2018
Available online 09 August 2018
1463-5003/

Table 1
Previous estimates of the global integral of the wind work (TW) on the geostrophic currents ($\overline{\tau \cdot V_g}$). The equatorial region (within ± 3° of the equator) is omitted from the calculation.

	Wunsch (1998)	Huang et al. (2006)	Hughes and Wilson (2008)
$\overline{\tau \cdot V_g}$	0.88	0.84	0.76

Table 2
Previous estimates of the global integral of the wind work (TW) on the ageostrophic currents ($\overline{\tau \cdot V_{ag}}$).

	Alford (2003) plus Wang and Huang (2004)	Huang et al. (2006)	Von Storch et al. (2007)
$\overline{\tau \cdot V_{ag}}$	2.8	0.3	2.7

Reanalysis, Huang et al. (2006) estimated the 10-year average (1993–2003) W_g as 0.84 TW (Table 1), consistent with Wunsch (1998). Hughes and Wilson (2008) estimated 0.76 TW (Table 1) total global W_g using 7-day averaged QuickSCAT scatterometer data and geostrophic surface currents calculated from a combination of satellite altimetry and surface drifter data. QuickSCAT directly measures wind stress and thus implicitly includes the effect of ocean surface currents in the wind stress measurements. This is different from the NCEP wind stress used in Wunsch (1998), which does not take into account the ocean surface currents. Duhaut and Straub (2006) found that wind work on the geostrophic currents was reduced by 20% when ocean surface currents dependency is considered in the wind stress formulation. To be consistent with Wunsch (1998), an additional 0.19 TW of wind work was added to their original wind work estimate to account for the reduction due to the effect of ocean currents (Hughes and Wilson, 2008). Therefore, their total of 0.95 TW is slightly larger than the estimate by Wunsch (1998) and Huang et al. (2006). To understand the effect of wind averaging frequency on W_g, Zhai et al. (2012) estimated W_g using 7-day averaged surface geostrophic currents and wind stress derived from 6-hourly, daily, and monthly NCEP winds. They found that wind work on geostrophic currents was increased by more than 70% when 6-hourly winds are used to calculate wind stress instead of monthly mean winds.

Numerical model output has been used to estimate the global W_g. Such estimates include Wunsch (1998), Huang et al. (2006), and Von Storch et al. (2007). All three studies give similar results range from 0.84 to 1.06 TW. Scott and Xu (2009) recognized that all these numerical studies used NCEP wind stress and thus studied the uncertainties associated with wind stress products finding it to be the dominant source of error. Their results suggested that ignoring the surface currents in the wind stress formulation can lead to an overestimate of W_g by 10 to 30%, a similar finding as Duhaut and Straub (2006). Zhai et al. (2012) found even larger overestimation of W_g by ~50% when surface currents in the wind stress formulation are omitted.

1.2. Previous estimates of wind work on surface ageostrophic currents

The ageostrophic current consists of the Ekman currents, produced by slowly varying and steady wind components, and near-inertial currents produced by high frequency winds. The wind work on the near-inertial motions has been described using a damped slab mixed layer model (D'Asaro, 1985; Alford, 2001; Watanabe and Hibiya, 2002; Alford, 2003). It was estimated to be 0.5 TW by Alford (2003). Wang and Huang (2004) developed a simple one dimensional (1D) model using the classical Ekman spiral. They estimated the average global wind work input into the surface Ekman currents to be 2.3 TW over a 54-year period (1948–2002) using the daily averaged wind stress data from the NCEP-NCAR reanalysis. When adding the numbers from these two studies together, we get the total wind work on surface ageostrophic currents (W_{ag}) to be 2.8 TW (Table 2).

Since ocean general circulation models (OGCM) can simulate both Ekman and near-inertial currents, they are widely used to estimate wind work on surface ageostrophic currents (W_{ag}). However, the results vary significantly among different studies due to their choice of model resolution, wind forcing, and averaging time scales. Using the daily mean surface currents from numerical simulations forced with daily mean wind stresses, Huang et al. (2006) estimated that the wind work on the ageostrophic surface currents was only 0.3 TW (Table 2), much smaller than the 2.8 TW estimated above. The spatially averaged thickness of the first layer in their numerical model is about 30 m and the horizontal resolution is 1° × 1°. Von Storch et al. (2007), on the other hand, reported a 2.7 TW (Table 2) of wind work on the ageostrophic surface currents using data from the OGCM for the Earth Simulator (OFES) at much finer vertical (5 m in first layer) and horizontal (0.1°) resolution. However, the OFES output was stored as snapshots on every third day and a daily averaged wind stress was applied to the numerical model.

1.3. Uncertainties of the wind work estimation on surface ageostrophic currents

As discussed in Section 1.2, there is an order of magnitude difference in previous estimate of the wind work on ageostrophic currents (Table 2) from 0.3 TW (Huang et al., 2006) to 2.7 TW (Von Storch et al. 2007) and 2.8 TW that is the sum of the estimates of Alford (2003) and Wang and Huang (2004). One reason is that neither Huang et al. (2006) nor Von Storch et al. (2007) have sufficient wind stress frequency to resolve the near-inertial currents at latitudes higher than 10°. But since the wind work on the near-inertial currents was estimated to be 0.5 TW (Alford 2003), most of the discrepancy comes from the wind work on the Ekman currents.

From the theoretical point of view, Wang and Huang (2004) suggested that they may underestimate the wind work on the Ekman currents because the classical Ekman spiral predicts an angle of 45° to the right (left) of wind stress in the Northern (Southern) Hemisphere, while field measurements find that the angle between the wind stress and surface drifter velocity is between 5° and 20° (Cushman-Roisin, 1994). Assuming the same Ekman depth in their 1D model and replacing the 45° surface angle used by Wang and Huang (2004) with 5°–20° angles, the wind work would increase by 33%–41% from 2.3 TW to 3.1–3.2 TW. Additionally, their estimate is also very sensitive to the calculation of the Ekman depth D_e. The authors chose an empirical formula (their Eq. 15 as shown below) to calculate D_e,

$$D_e = \gamma \frac{u_*}{f}, \tag{6}$$

where $u_*$is the frictional velocity, f is the Coriolis parameter, and γ is an empirical constant set to be 0.5 determined through a best fit of six sets of observations (Wang and Huang, 2004, their Fig. 2). Their estimate of γ is higher than commonly used values ($\gamma \approx 0.25 - 0.4$). If we take the 5°–20° angle and vary the γ value, the wind work estimate will change to 3.8–4.1 TW if $\gamma = 0.4$ is used and it is doubled if $\gamma = 0.25$ is used.

For the numerical studies, the surface current is not the current on sea surface (z = 0) but rather the vertical average of the currents in the first layer of the OGCM. The choice of first layer thickness in the model greatly affects the magnitude of the Ekman currents used in the wind work estimations. Assuming the diffusivity is vertically constant and taking the direction of τ as the x-axis, the classical solution of Ekman spiral is

$$U_e = \frac{\sqrt{2}\tau}{\rho_o f D_e} e^{z/D_e} \cos\left(\frac{z}{D_e} - \frac{\pi}{4}\right), \tag{7}$$

where U_e is the Ekman velocity along the x direction, ρ_o is the density of

the ocean, and z is the vertical coordinate. Since the cross-wind Ekman current component does not contribute to the wind work, we only need to integrate the along wind component U_e in the first model layer:

$$\int_{-\Delta z}^{0} U_e dz = \frac{\sqrt{2}\tau}{\rho_o f} e^{-\Delta z/D_e} \sin\left(\frac{\Delta z}{D_e}\right), \tag{8}$$

where Δz is the thickness of the first layer. Thus, the ratio of the depth-average U_e in the first model layer (U_{elayer}) to the U_e at the ocean surface is

$$\frac{U_{elayer}}{U_e(z=0)} = \frac{D_e}{\Delta z} e^{-\frac{\Delta z}{D_e}} \sin\left(\frac{\Delta z}{D_e}\right). \tag{9}$$

Previous studies have suggested that the surface Ekman layer extends only about 10–20 m deep. Price et al. (1987) estimated $D_e = 12$ m defined by the depth of the e-folding scale of the amplitude of the surface ageostrophic currents in the western Sargasso Sea. Chereskin (1995) suggested a similar value of $D_e = 18$ m in the California Current, and a 22 m Ekman depth in Drake Passage was reported by Lenn and Chereskin (2009). Numerical models with the first layer thickness of 5 (Von Storch et al., 2007), 10 (Von Storch et al., 2012), and 30 m (Huang et al., 2006) underestimate the surface Ekman current along the wind stress direction and thus the wind work on the surface Ekman currents by 42% (23%), 69% (42%), and 100% (85%), respectively when the Ekman depth is 10 m (20 m).

Furthermore, Wang and Huang (2004, their Eq. 14 as shown below) suggested that wind work on surface Ekman currents generated by the variational wind stress is

$$W_e = \sum_{-\infty}^{\infty} \frac{1}{\rho_o D_e} \left(\frac{1}{|f(f+\omega_n)|}\right)^{1/2} T_n^2, \tag{10}$$

where ω_n and T_n are the frequency and magnitude of the nth component of the wind stress, respectively. Thus, all the three previous estimates of wind work on Ekman currents (Wang and Huang, 2004; Huang et al., 2006; Von Storch et al., 2007) lack the contribution from components with frequencies higher than the daily resolution of wind stress since they all utilized daily averaged wind stress forcing.

1.4. Goals of this study

In this study, we calculate the wind work (W) input to the global surface currents using model output from a 17-year global HYbrid Coordinate Ocean Model (HYCOM) reanalysis. This research differs and improves on previous studies in that (1) the model surface layer has a thickness of 1 m and thus the ocean surface Ekman currents are better represented; (2) the reanalysis is forced by hourly surface stress and thus is able to fully resolve near-inertial currents in high latitudes and capture the wind work on surface Ekman currents from the high frequency wind stress variations; and (3) the reanalysis provides more realistic sea surface height (SSH) fields and thus more accurate surface currents than non-data assimilative simulations.

Note that in the real ocean, surface gravity waves play an important role in redistributing momentum and energy in the water column through wave breaking and Langmuir turbulence. Large eddy simulation studies have shown that both wave breaking and Langmuir turbulence reduce the mean vertical velocity shear near the surface with the influence of surface gravity waves on the Ekman layer (McWilliams et al., 1997, 2012). However, OGCMs (including HYCOM used in this study) usually apply a mean surface wind stress that varies smoothly in space and time on scales much greater than those of the surface gravity waves. High-frequency and small-scale motions generated by breaking waves and Langmuir turbulence are naturally filtered out by the grid resolution of the OGCMs. Even though the 1 m thick surface layer in HYCOM can provide a better representation of the surface currents than the 5–30 m surface layer thicknesses in the other models mentioned in Section 1.3, the surface gravity waves are not part of the model physics in any of these systems.

The reanalysis output contains hourly instantaneous surface currents, surface stress, and SSH fields. This provides an opportunity to estimate both wind work on the surface geostrophic and ageostrophic currents. We are especially interested in the total wind work on ageostrophic currents ($\overline{\boldsymbol{\tau}\cdot\boldsymbol{V_{ag}}}$) since the uncertainty of the previous estimates is large. Although the wind stress formulation used in this HYCOM reanalysis takes into account the ocean surface currents (Pacanowski, 1987; Luo et al., 2005; Duhaut and Straub, 2006; Hughes and Wilson, 2008; Xu and Scott, 2008; Yu et al., 2017), the global wind work difference due to the wind stress formulation with or without ocean surface currents is not the focus of this research and beyond the scope of this study.

This paper is organized as follows: Section 2 describes the numerical model and data assimilation for the reanalysis. The wind work on surface geostrophic currents is validated against previous studies in Section 3. The reanalysis results of wind work on ageostrophic currents are presented in Section 4, which is followed by discussion and conclusions in Section 5.

2. Numerical model and simulation

A 17-year global HYCOM reanalysis from 1999 to 2015 is used for this study. HYCOM is widely used in the ocean community (http://www.hycom.org) and is the ocean model component for the present operational US Navy Global Ocean Forecast System (Metzger et al., 2014). It has been applied to large scale, marginal seas, and coastal studies. HYCOM is a primitive equation general ocean circulation model and solves five prognostic equations: two horizontal velocity components, mass conservation, temperature and salinity conservation. A detailed description of HYCOM physics is provided by Bleck (2002). HYCOM is briefly presented below with emphasis on the numerical aspects that are relevant to this study. There are no tides or surface waves in this reanalysis.

2.1. Model outputs, grids

The HYCOM horizontal resolution in this study is 0.08° (1/12.5°) that is ~9 km at the equator and ~6.5 km at mid-latitude making it globally eddy-resolving. The grid is uniform cylindrical from 78.64°S-66°S, Mercator between 66°S-47°N and includes a bipolar patch north of 47°N providing ~3.5 km grid spacing at the North Pole. There are 41 hybrid (z, sigma, and isopycnal) coordinate layers vertically with potential density referenced to 2000 m. The first vertical layer has a uniform layer thickness of 1 m.

For the output, hourly instantaneous surface stress, surface current velocities, and SSH fields are interpolated to a uniform 0.08° resolution between 40°S-40°N and to 0.04° resolution poleward of these latitudes. The ocean surface geostrophic currents are calculated from SSH fields assuming geostrophic balance. The ageostrophic currents are the difference between the surface currents and the geostrophic currents.

2.2. Data assimilation

The data assimilation technique employed for the reanalysis is a three dimensional (3D) variational scheme used within the Navy Coupled Ocean Data Assimilation (NCODA) (Cummings 2005; Cummings and Smedstad, 2013). Available remotely sensed sea surface temperature (SST), SSH, sea ice concentration, and in-situ observations of temperature and salinity from profiles, ships, and moored and drifting buoys are all assimilated into HYCOM. NCODA also generates synthetic temperature and salinity profiles for assimilation that are formed from the two dimensional SSH and SST using a 3D synthetic profile method, the Improved Synthetic Ocean Profile (Helber et al., 2013).

2.3. Initialization and surface forcing

The 17-year reanalysis is separated into one 3-year stream starting in 1999, six 2.5-year streams starting in 2001, and one 3-year stream from 2013 to 2015. For each stream, the initialization state comes from a previous 20-year ocean reanalysis (Thoppil et al., 2015; Yu et al., 2015) on December 1 of the previous year except the very first stream started in June 1998.

Atmospheric forcing for this reanalysis is from the 0.3125° hourly NCEP Climate Forecast System Reanalysis (CFSR) (Saha et al., 2010). The wind stress formulation in the model includes the ocean surface currents. The NCEP CFSR 10-m wind velocities are read by HYCOM and the surface stress is calculated at every time step taking into account the ocean surface currents. The surface stress in the previous 20-year ocean reanalysis used to initialize the model does not include the ocean surface currents in the wind stress formulation. When the new wind stress formulation (include ocean surface current) is applied to the model, the mesoscale eddy field adjusts to the satellite altimeter data within the first month (Yu et al., 2015) but the basin wide kinetic energy takes another 6 months to reach "equilibrium". Thus, while the ~2.5-year streams start on December 1 of the previous year and end after 31 months of integration, i.e. the end of June, only the last two years of output (i.e. July 2001–June 2003) from each ~2.5-year stream are used in the analysis here. Reanalysis data from January 1999 to June 2001 in the first stream and from July 2013 to December 2015 in the last stream are used in the analysis.

3. Wind work on geostrophic currents

In this study, the overbar terms in Eqs. (1)–(5) are 17-year averages and the prime terms are eddy components relative to the 17-year average of ocean currents and wind stress. All figures are presented in the latitude range from 80°S to 80°N, while global integrals are given in the region between 63°S and 63°N to be consistent with previous studies. A detailed description of the wind work terms in Eq. (4) is given in this section.

3.1. The mean part of the 17-year average wind work on the surface geostrophic currents ($\overline{\tau}\cdot\overline{\mathbf{V}_g}$)

The 17-year average mean wind stress ($\overline{\tau}$) and geostrophic currents ($\overline{\boldsymbol{V}_g}$) are used to calculate the mean part of the wind work on the surface geostrophic currents. To be consistent with Wunsch (1998), the equatorial region (within ± 3° of the equator) is omitted from these calculations. The two components ($\overline{\tau_x}\,\overline{u_g}$ and $\overline{\tau_y}\,\overline{v_g}$) of $\overline{\boldsymbol{\tau}}\cdot\overline{\boldsymbol{V}_g}$ are shown in Fig. 1a and c, respectively. The global (63°S–63°N to be consistent with Wunsch, 1998) integral (Table 3) shows the dominance of $\overline{\tau_x}\,\overline{u_g}$ (0.78 TW) relative to $\overline{\tau_y}\,\overline{v_g}$ (0.03 TW), which are 0.02 and 0.01 TW smaller than the Wunsch (1998) estimate, respectively. This is due to the inclusion of surface current in the wind stress formulation in our model that reduces the wind work (Duhaut and Straub, 2006). Please note that the two decimal points do not imply an absolute accuracy of 0.01 TW, but are given to allow a comparison with the numbers of the same order by Wunsch (1998).

The spatial patterns are very similar to that found in previous studies (Wunsch, 1998; Von Storch et al., 2007; Hughes and Wilson, 2008; Scotts and Xu, 2009; Zhai et al., 2012). The most significant positive input of $\overline{\tau_x}\,\overline{u_g}$ comes from the Antarctic Circumpolar Current (ACC) in the Southern Ocean, the Gulf Stream, the Kuroshio (Wunsch, 1998), and the Caribbean Current (Hughes and Wilson, 2008). Seventy one percent of the global integral of $\overline{\tau_x}\,\overline{u_g}$ occurs to the south of 40°S due to the persistent strong winds above the ACC that is the world's strongest current system (Fig. 1b). The most significant negative values of $\overline{\tau_x}\,\overline{u_g}$ are found over the North Equatorial Countercurrent (Fig. 1a and b), which is the same as Hughes and Wilson (2008, their Fig. 1). Twenty one percent of the global integral of $\overline{\tau_x}\,\overline{u_g}$ comes from tropical-subtropical regions within ± 20° of the equator. Notice that although the Gulf Stream and Kuroshio have their strong signatures in the global pattern (Fig. 1a), their contributions to $\overline{\tau_x}\,\overline{u_g}$ are small when integrated zonally (Fig. 1b). This is because the ocean surface areas occupied by both current systems are small, and thus their contributions are smeared out by the zonal integration. $\overline{\tau_y}\,\overline{v_g}$ (Fig. 1c) is much smaller than $\overline{\tau_x}\,\overline{u_g}$, and 91% of the wind work occurs within ± 20° of the equator (Fig. 1d). The total mean component of the wind work on geostrophic currents ($\overline{\boldsymbol{\tau}}\cdot\overline{\boldsymbol{V}_g}$, Fig. 1e) thus follows closely the spatial distribution of $\overline{\tau_x}\,\overline{u_g}$ (Fig. 1a). Its global integral is 0.81 TW with 69% of the wind work occurring to the south of 40°S and another 23% occurring within ± 20° of the equator (Fig. 1f).

3.2. The eddy part of the 17-year average wind work on the surface geostrophic currents ($\tau'\cdot\mathbf{V}_g'$)

To calculate $\boldsymbol{V}_g'$, we first calculate 10-day average SSH from the hourly SSH outputs and then the 10-day average geostrophic current $\boldsymbol{V}_g$ is calculated assuming geostrophic equilibrium following Wunsch (1998). $\boldsymbol{V}_g'$ is the difference between the 10-day average geostrophic current and the 17-year average geostrophic current. The surface stress is also averaged every 10-day period to calculate $\boldsymbol{\tau}'$.

Unlike the mean part, both components ($\overline{\tau_x'u_g'}$ and $\overline{\tau_y'v_g'}$) of $\overline{\boldsymbol{\tau}'\cdot\boldsymbol{V}_g'}$ show similar magnitude, and their spatial patterns (Fig. 2a and c) are very similar to Wunsch (1998). The most dominant positive contribution comes from the tropics and the most dominant negative values occur in the Southern Ocean (Fig. 2a–d). Like Wunsch (1998), the reanalysis results also show significant positive and negative contributions in the western monsoon region of the Indian Ocean. The global integral of $\overline{\tau_x'u_g'}$ and $\overline{\tau_y'v_g'}$ in our calculation is −0.042 and −0.057 TW (Table 4), respectively, in comparison to 0.029 and 0.01 TW in Wunsch (1998). These differences mainly come from the high mesoscale eddy activity regions: south of 40°S, the Agulhas Current, the Kuroshio Extension, and the Gulf Stream.

Duhaut and Straub (2006) pointed out that the reduction of geostrophic wind work due to the surface currents in the wind stress formulation is the strongest in regions of high mesoscale eddy activity. Hughes and Wilson (2008) further show that more than 75% of this effect is represented by $\overline{\boldsymbol{\tau}'\cdot\boldsymbol{V}_g'}$. Thus, the negative values of $\overline{\boldsymbol{\tau}'\cdot\boldsymbol{V}_g'}$ (Fig. 2a and c) found in the Southern Ocean, the Agulhas Current, the Kuroshio Extension, and the Gulf Stream can be attributed to the effect of including ocean surface currents in the wind stress formulation, which is not included in Wunsch (1998).

The spatial distribution of $\overline{\boldsymbol{\tau}'\cdot\boldsymbol{V}_g'}$ and its zonal integral are shown in Fig. 2e and f. They look very similar to Fig. 5a in Hughes and Wilson (2008), which also contains the effect of ocean currents in their wind stress formulation. There are strong positive and negative contributions in the tropics with positive contributions dominating and strong negative contributions in the regions with strong mesoscale eddy activity. However, a closer inspection reveals that our results have a systematic low bias in comparison with Hughes and Wilson (2008). The integral between 20°S and 20°N in our model is 0.027 TW that is smaller than the Hughes and Wilson (2008) 0.039 TW estimate. In our zonal integration (Fig. 2f), the magnitude of negative contributions from the Southern Hemisphere around 40°S is larger than the maximum positive contribution around 10°N (Fig. 2f), which is opposite to the findings by Hughes and Wilson (2008, their Fig. 5a). Our total integral south of 20°S is −0.103 TW, quadruple the integral of −0.026 TW for the same region in Hughes and Wilson (2008, their Table 3). The global integral of $\overline{\boldsymbol{\tau}'\cdot\boldsymbol{V}_g'}$ of the reanalysis is −0.099 TW compared with 0.009 TW in Hughes and Wilson (2008) and 0.039 TW in Wunsch (1998).

There are two possibilities that can contribute to these differences. The first is that the reduction of geostrophic wind work due to the surface currents via the wind stress is probably diluted in Hughes and Wilson (2008). In order to be able to fully resolve the effect of ocean

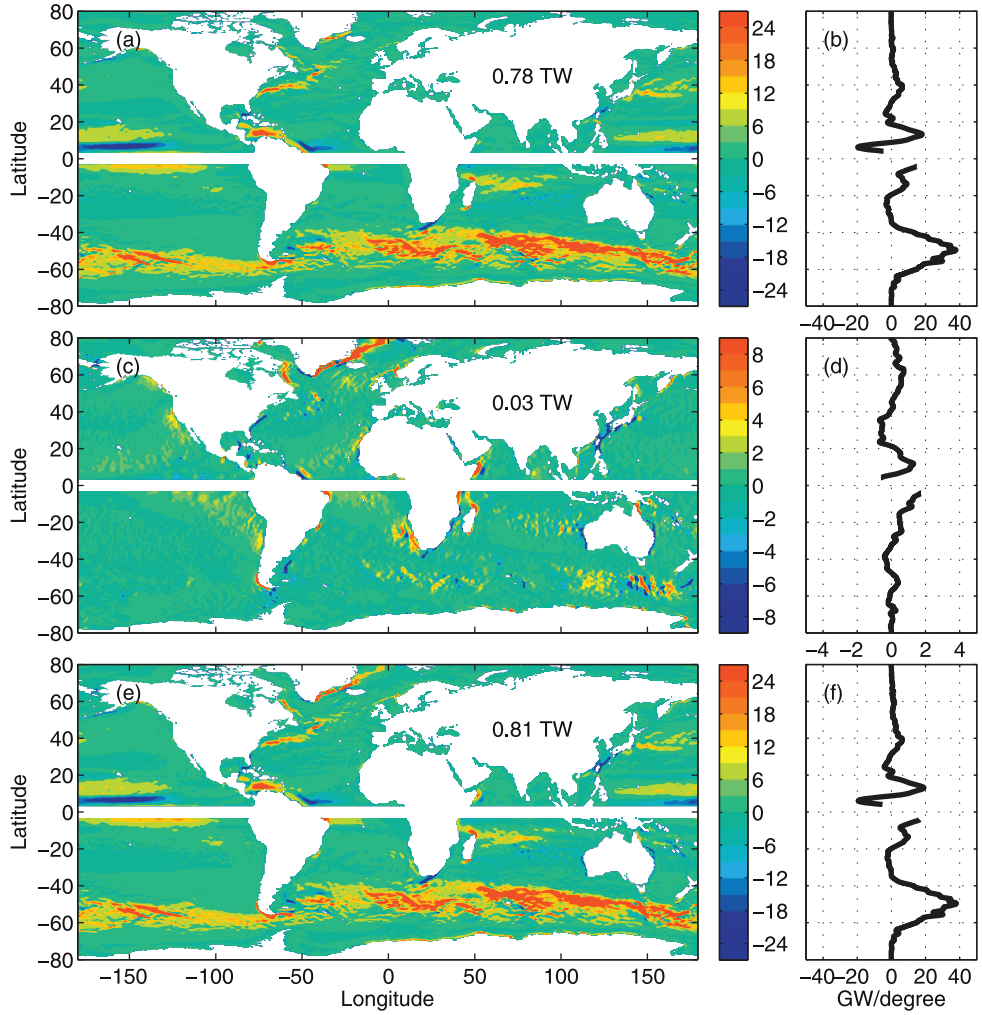

Fig. 1. Seventeen-year average (10^{-3} W/m^2) of (a) $\overline{\tau_x u_g}$, (c) $\overline{\tau_y v_g}$, and (e) $\overline{\tau \cdot V_g}$ over the period 1999–2015, and the corresponding meridional distribution of the zonal integral (b), (d), and (f), respectively. The global wind work integral is noted over Asia for all figures. Note the range of the color bar is different for some panels on this figure and on subsequent figures.

Table 3
Global integral (63°S - 63°N) of the mean part of the wind work (TW) on the eastward ($\overline{\tau_x u_g}$), northward ($\overline{\tau_y v_g}$) geostrophic currents components, and the ageostrophic currents ($\overline{\tau \cdot V_{ag}}$). The equatorial region (within ± 3° of the equator) is omitted from the calculation.

Component	$\overline{\tau_x u_g}$	$\overline{\tau_y v_g}$	$\overline{\tau \cdot V_{ag}}$
HYCOM reanalysis	0.78	0.03	1.28

currents on wind work via wind stress formulation, the wind stress and current measurements need to be matched well-enough in time and space for the mesoscale features in both currents and wind stresses field to be aligned. It is possible that this requirement was not met for observations (Hughes and Wilson, 2008). The second possibility comes from the spatial resolution of the available data. As mentioned in Section 2.1, the horizontal resolution of the HYCOM reanalysis is eddy resolving at 0.08°. The data used by Wunsch (1998) were gridded at 2° resolution which is not able to resolve mesoscale eddies. The data used by Hughes and Wilson (2008) were gridded on a 1/3° Mercator grid, which is eddy permitting, but not able to fully resolve the mesoscale eddies properly. Thus, the spatial resolution of available data may limit Hughes and Wilson (2008) from fully capturing the contribution of mesoscale eddies on $\overline{\tau' \cdot V_g'}$. And the decreasing trend of $\overline{\tau' \cdot V_g'}$ (0.039, 0.009, −0.099 TW) with the increase of the spatial resolution among the three studies supports this assumption.

3.3. The 17-year average wind work on the surface geostrophic currents ($\overline{\tau \cdot \mathbf{V}_g}$)

Both the spatial pattern (Fig. 3a) and its zonal integral (Fig. 3b) of the 17-year average total wind work on the surface geostrophic currents ($\overline{\tau \cdot V_g}$) agree well with Hughes and Wilson (2008). The most dominant contribution comes from the Southern Ocean, which accounts for 70% of the total wind work on the geostrophic currents. The global integral is 0.71 TW, 19% less than the estimate of 0.88 TW in Wunsch (1998) and 7% less than the 0.76 TW estimate in Hughes and Wilson (2008). Among the 0.17 TW reduction compared to the Wunsch (1998), 0.14 TW (82%) comes from $\overline{\tau' \cdot V_g'}$. This clearly supports the idea that most of the reduction of $\overline{\tau \cdot V_g}$ by including the ocean currents in the wind stress formulation comes from the eddy part ($\overline{\tau' \cdot V_g'}$) of the wind work (Duhaut and Straub, 2006; Hughes and Wilson, 2008).

4. Wind work on ageostrophic currents

The hourly ageostrophic currents are calculated as the difference

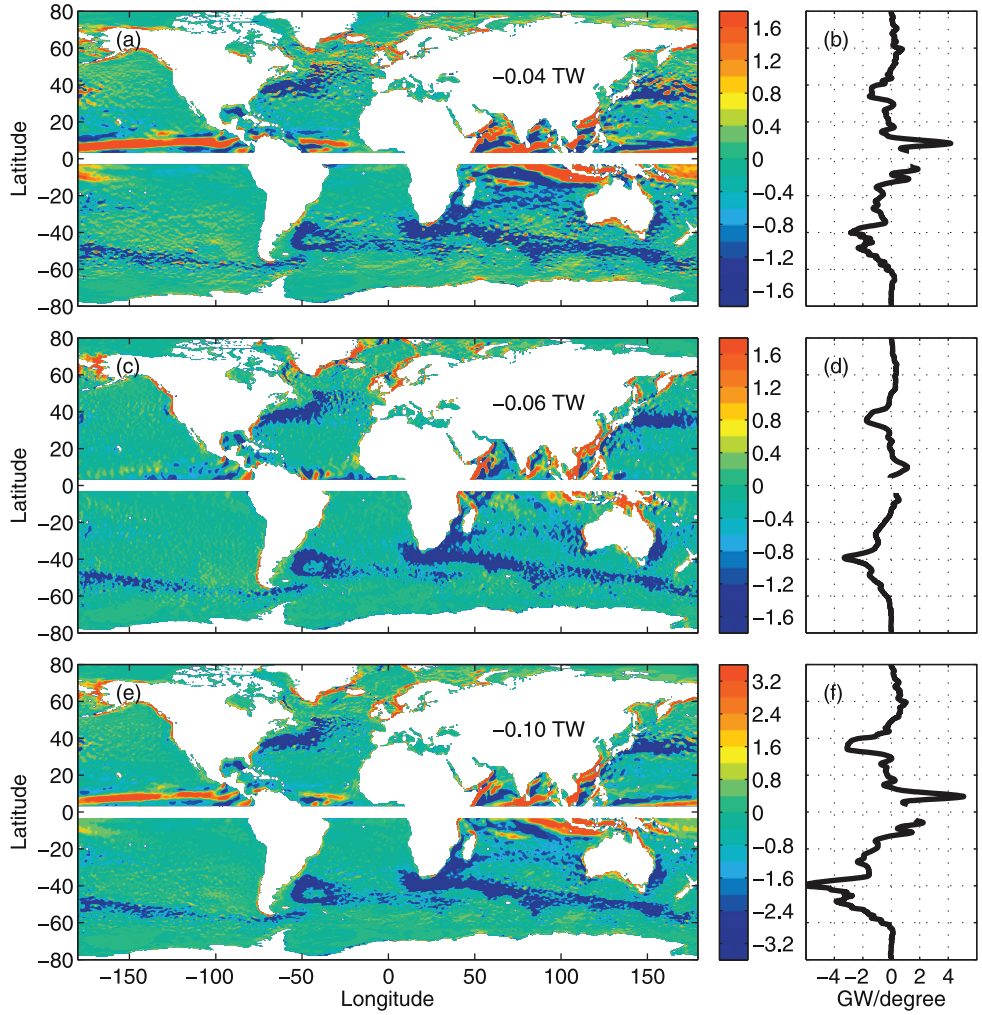

Fig. 2. Seventeen-year average (10^{-3} W/m^2) of (a) $\overline{\tau_x' u_g'}$, (c) $\overline{\tau_y' v_g'}$, and (e) $\overline{\tau' \cdot V_g'}$ ($\overline{\tau_x' u_g'} + \overline{\tau_y' v_g'}$) over the period 1999–2015 calculated from 10-day average outputs, and the corresponding meridional distribution of the zonal integral (b), (d), and (f), respectively.

Table 4
Global integral (63°S - 63°N) of the eddy part of the wind work (TW) on the eastward ($\overline{\tau_x' u_g'}$), northward ($\overline{\tau_y' v_g'}$) geostrophic currents components, and the ageostrophic currents ($\overline{\tau' \cdot V_{ag}'}$). The equatorial region (within ± 3° of the equator) is omitted from the calculation.

Component	$\overline{\tau_x' u_g'}$	$\overline{\tau_y' v_g'}$	$\overline{\tau' \cdot V_{ag}'}$
HYCOM reanalysis	−0.042	−0.057	4.15

between the hourly surface currents and the corresponding 10-day average surface geostrophic currents. The sensitivity of the wind work on the ageostrophic currents to the choice of different geostrophic average periods is discussed in Section 5.1. The 17-year average ageostrophic currents are calculated as the difference between the 17-year average surface currents and surface geostrophic currents.

4.1. The mean part of the 17-year average wind work on the ageostrophic currents ($\overline{\tau} \cdot \overline{\mathbf{V}_{ag}}$)

The 17-year average mean wind stress ($\overline{\tau}$) and ocean surface ageostrophic currents ($\overline{V_{ag}}$) are used to calculate the mean part of the wind work on the ageostrophic currents. Since the 17-year average ageostrophic currents are surface Ekman currents, classical theory tells us that the mean part of the wind work on the surface Ekman currents (Wang and Huang, 2004) is

$$\overline{\tau} \cdot \overline{V_{ag}} = \frac{\overline{\tau}^2}{\rho_o f D_e}. \tag{11}$$

We should expect a high correlation between $\overline{\tau} \cdot \overline{V_{ag}}$ and the magnitude of the mean wind stress. Indeed, the spatial distribution of $\overline{\tau} \cdot \overline{V_{ag}}$ (Fig. 4a) in our model is very similar to the mean wind stress magnitude (Fig. 5a) with a high correlation coefficient of 0.95.

The global integral of $\overline{\tau} \cdot \overline{V_{ag}}$ is 1.28 TW (Table 3). Its main contribution comes from two regions with the largest contribution (47%) from the Southern Ocean south of 40°S (Fig. 4a and b) due to the strong currents driven by strong wind stress, and the second largest contribution (35%) from the tropical-subtropical region within ± 20° of the equator.

4.2. Comparing $\overline{\tau} \cdot \overline{\mathbf{V}_{ag}}$ with Wang and Huang (2004)

The 1.28 TW global integral of $\overline{\tau} \cdot \overline{V_{ag}}$ is in decent agreement with the Von Storch et al. (2007) 1.06 TW estimate but more than double the Wang and Huang (2004) 0.54 TW estimate. However, the 75% contribution from the Southern Hemisphere in our calculation is almost the same as the 74% estimate in Wang and Huang (2004).

To understand the magnitude difference between the reanalysis and Wang and Huang (2004), $\overline{\tau} \cdot \overline{V_{ag}}$ is also estimated theoretically in the same way as Wang and Huang (2004, their Eqs. 15 and 13) by applying the 17-year average surface stress to Eqs. (6) and (11). The spatial distribution of the theoretical estimate Fig. 5b) is very similar to what's

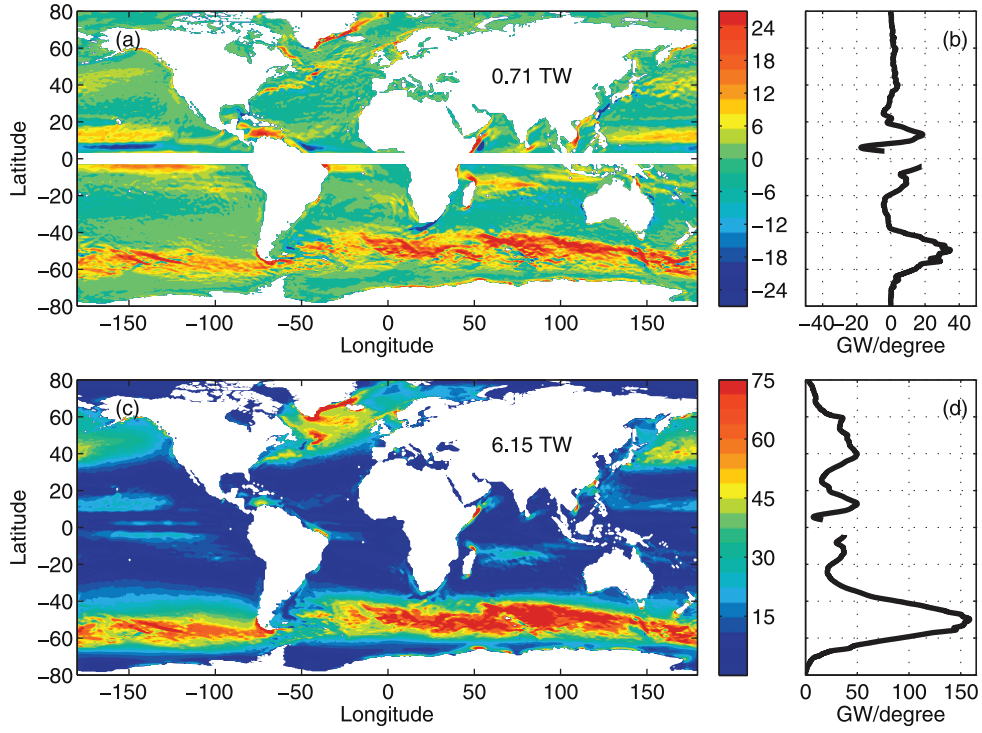

Fig. 3. Seventeen-year average (10^{-3} W/m^2) of (a) $\overline{\tau \cdot V_g}$ over the period 1999–2015 calculated from 10-day average outputs, (b) the corresponding meridional distribution of the zonal integral of $\overline{\tau \cdot V_g}$, (c) $\overline{\tau \cdot V}$ calculated from hourly average outputs, and (d) the corresponding meridional distribution of the zonal integral of $\overline{\tau \cdot V}$.

calculated from the reanalysis data (Fig. 4a) with a high spatial correlation of 0.97. The meridional variation of the zonal integral (Fig. 5c) is also in good agreement with the reanalysis (Fig. 4b). But the wind work magnitude of the theoretical estimate is much smaller with a 0.46 TW global integral, which is in much better agreement with the Wang and Huang (2004) 0.54 TW estimate. Kelly et al. (2001) find that including surface currents in the wind stress formulation reduces the wind stress magnitude. Thus, the 0.08 TW difference between our theoretical estimate and Wang and Huang (2004) can mainly be attributed to the smaller surface stress in the reanalysis induced by the inclusion of surface currents in the wind stress formulation. Since the choice of wind stress data only makes a very small difference in the estimate of $\overline{\tau} \cdot \overline{V_{ag}}$ using the same method, the large difference (1.28 vs 0.54 TW) between the reanalysis and Wang and Huang (2004) resides in their usage of Eqs. (6) and (11) to estimate the wind work vs the internal physics in HYCOM.

Eq. (11) is derived from the classical Ekman spiral that predicts a constant 45° angle (Wang and Huang, 2004) between the surface Ekman current and wind stress. As can be seen from Fig. 5d, this angle varies significantly with location. In the Southern Ocean where most of the wind work occurs, the average angle (Fig. 5e) is 34°. According to our discussion in Section 1.3, the wind work calculated from the reanalysis can be 17% larger (cos 34/cos 45) than that calculated using the classical theory in this region assuming the same Ekman depth.

For a given mean wind stress dataset, the wind work is inversely proportional to the Ekman depth (Eq. (6)) according to Eq. (11). The Wang and Huang (2004) estimation will be doubled to 1.08 TW if $\gamma = 0.25$ is used in Eq. (6). And their estimate can be further increased to 1.26 TW when we consider the angle difference in the Southern Ocean, which is in close agreement with our 1.28 TW estimate.

4.3. The eddy part of the 17-year average wind work on surface ageostrophic currents ($\tau' \cdot \mathbf{V}_{ag}$)

$\overline{\tau' \cdot V_g'}$ is much smaller than $\overline{\tau} \cdot \overline{V_g}$, but $\overline{\tau' \cdot V_{ag}'}$ (Fig. 4c) is much larger than $\overline{\tau} \cdot \overline{V_{ag}}$ (Fig. 4a). The global (63°S - 63°N) integral of $\overline{\tau' \cdot V_{ag}'}$ is 4.15 TW (Table 4) and is more than double the 1.83 TW estimated by Wang and Huang (2004). Despite the large magnitude difference, both estimates of $\overline{\tau' \cdot V_{ag}'}$ show 60% of the corresponding contribution from the Southern Hemisphere.

$\overline{\tau' \cdot V_{ag}'}$ (Fig. 4c and d) is very strong over two regions: the Southern Ocean and the subpolar basins in the North Pacific and North Atlantic Oceans. The Southern Ocean to the south of 40°S contributes 43% to the global integral while the northern storm-track regions to the north of 30°N contributes another 26%. The eddy ageostrophic wind work is strong over the storm-track regions due to the strong synoptic wind variability and is in general small in the tropical-subtropical region (Fig. 4c). But the tropical Indian Ocean and South China Sea show moderate values of $\overline{\tau' \cdot V_{ag}'}$, probably due to monsoon activities in the regions.

4.4. Comparing $\overline{\tau \cdot \mathbf{V}_{ag}}$ with Wang and Huang (2004)

The spatial pattern (Fig. 4e) and its zonal integral (Fig. 4f) of $\overline{\tau \cdot V_{ag}}$ ($\overline{\tau} \cdot \overline{V_{ag}} + \overline{\tau' \cdot V_{ag}'}$) are very similar to these reported by Wang and Huang (2004, their Fig. 3) but with much larger magnitude. The three regions that make significant contributions to $\overline{\tau \cdot V_{ag}}$ in the reanalysis are consistent with Wang and Huang (2004), namely: 1) the ACC, 2) the storm track regions in the North Atlantic and North Pacific Oceans, and 3) the South China Sea and South Indian Ocean/Arabian Sea. Furthermore, despite the magnitude difference, the ratio of the Southern Hemisphere contribution (67%) to the global integral of $\overline{\tau \cdot V_{ag}}$ (5.44 TW) in the reanalysis is similar to the 63% estimate in Wang and Huang (2004). The difference of the global integral of these two estimates is 3.14 TW.

Part of the 3.14 TW wind work difference comes from the wind work on the near-inertial currents. The Nyquist frequency of the hourly surface stress forcing (0.5 cycles per hour) for the reanalysis is much higher than the inertial frequency in the global ocean. Thus, the reanalysis is capable of fully resolving the near-inertial currents while the Wang and Huang (2004) 2.3 TW estimate is wind work purely on

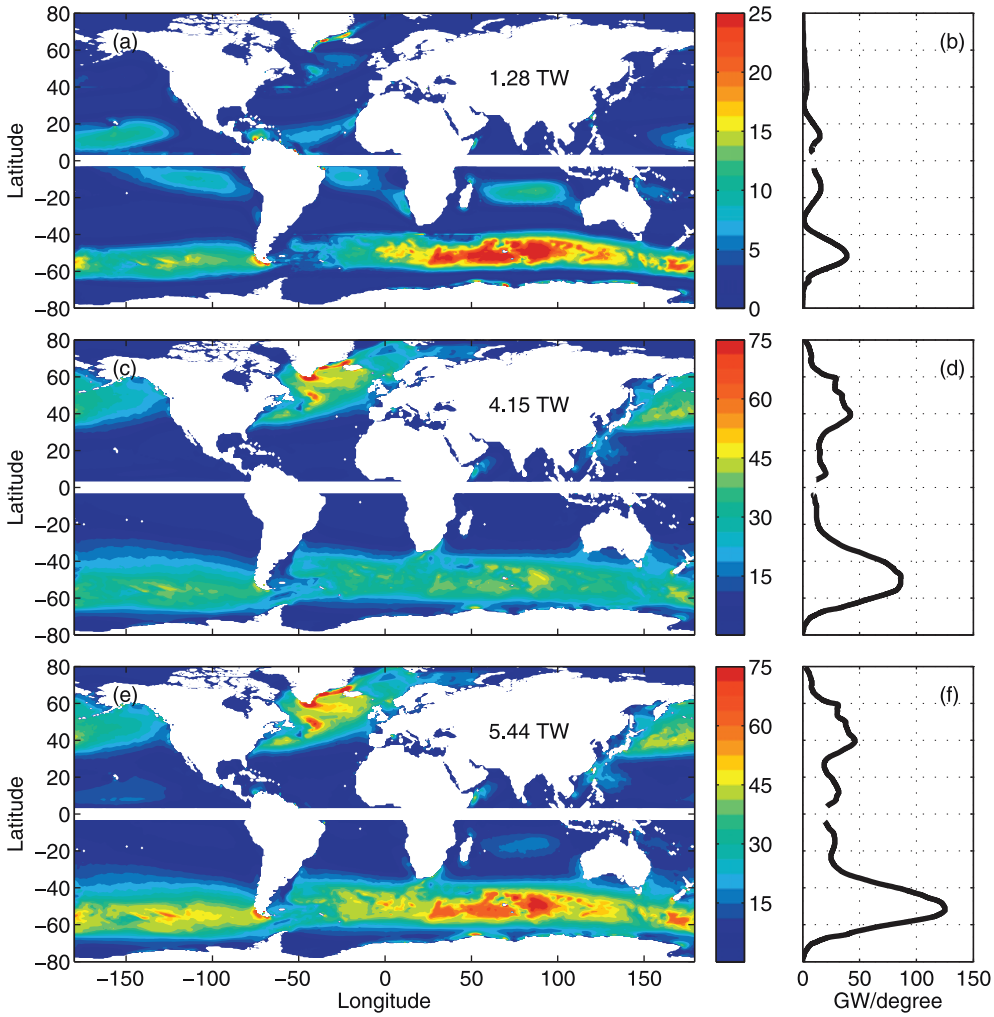

Fig. 4. Seventeen-year average (10^{-3} W/m^2) of (a) $\overline{\tau}\cdot\overline{\boldsymbol{V}_{\boldsymbol{ag}}}$, (c) $\overline{\tau'\cdot\boldsymbol{V}'_{ag}}$, and (e) $\overline{\tau\cdot\boldsymbol{V}_{\boldsymbol{ag}}}$ over the period 1999–2015 calculated from hourly reanalysis outputs, and the corresponding meridional distribution of the zonal integral (b), (d), and (f), respectively.

surface Ekman currents. It would be the best if the wind work on the near-inertial currents can be calculated using the reanalysis output by temporally filtering the near-inertial surface stresses and currents. But this is not practical due to the memory limitations for the 17-year hourly time series of the global eddy resolving grid resolution (4500 × 3298). So, the 0.5 TW estimate from Alford (2003) is taken as a reference of the contribution of the global wind work on the near-inertial currents to the 3.14 TW wind work difference. The 0.6 TW estimate from Watanabe and Hibiya (2002) is 20% larger than the estimate of Alford (2003), but it doesn't change our conclusions.

The 3.14 TW wind work difference can also be partially explained by the frequency difference of wind stress used in the two estimates, with hourly wind stress in the reanalysis being much higher than the daily wind stress used in Wang and Huang (2004). To quantify this effect, we calculate the wind work on the ageostrophic currents with the daily averaged outputs to be consistent with Wang and Huang (2004). Its spatial pattern and zonal integral Fig. 6a and b) are very similar to the hourly results (Fig. 4e and f) and the global integral is 4.18 TW, 1.26 TW less than the hourly reanalysis results. The differences between these two estimates are shown in Fig. 6c and d. There are two regions that mainly contribute to this difference: the ACC and the storm track regions in the North Atlantic and North Pacific Oceans (Fig. 6c) since much of the time dependence of the wind stress in the tropics is seasonal whereas the time dependence of the wind stress at the mid-latitudes is more dominated by synoptic time scales (Von Storch et al., 2007; Zhai et al., 2012). The 1.26 TW global integral difference contains two parts: 1) the high frequency (daily to hourly) wind work contribution to the Ekman currents according to Eq. (10), and 2) the difference from the wind work on the near-inertial currents. The daily averaged reanalysis output is sufficient to resolve near-inertial currents within 10° of the equator, so the contribution of near-inertial current in this region cannot be reflected by this difference. Since Alford (2003, Fig. 1) suggests that 0.10 TW of the wind work on near-inertial currents comes within ± 10° of the equator and 0.40 TW in the remaining global ocean, we calculate that the wind work difference due to the high frequency wind stress (daily to hourly) variation on Ekman currents is 0.86 TW (1.26 TW–0.4 TW). In total, the wind stress frequency difference and the wind work on inertial currents together counts for 1.36 TW (0.86 TW + 0.5 TW) of wind work difference between the reanalysis and Wang and Huang (2004). The remaining 1.78 TW difference is likely coming from the over-estimate of Ekman depth and the constant 45° angle between wind stress and surface Ekman current in Wang and Huang (2004) as discussed in Section 4.2.

4.5. *Comparing* $\overline{\tau\cdot\mathbf{V}_{\mathbf{ag}}}$ *with Von Storch et al. (2007)*

Our total wind work on the surface ageostrophic currents is also much larger than the 2.7 TW estimated by Von Storch et al. (2007). The difference between the reanalysis and Von Storch et al. (2007) is likely due to three major reasons. First, the 1 m thickness of HYCOM's first layer allows it to represent 90% (95%) of the surface Ekman current when the Ekman depth is 10 (20) m whereas the 5 m thick first layer in

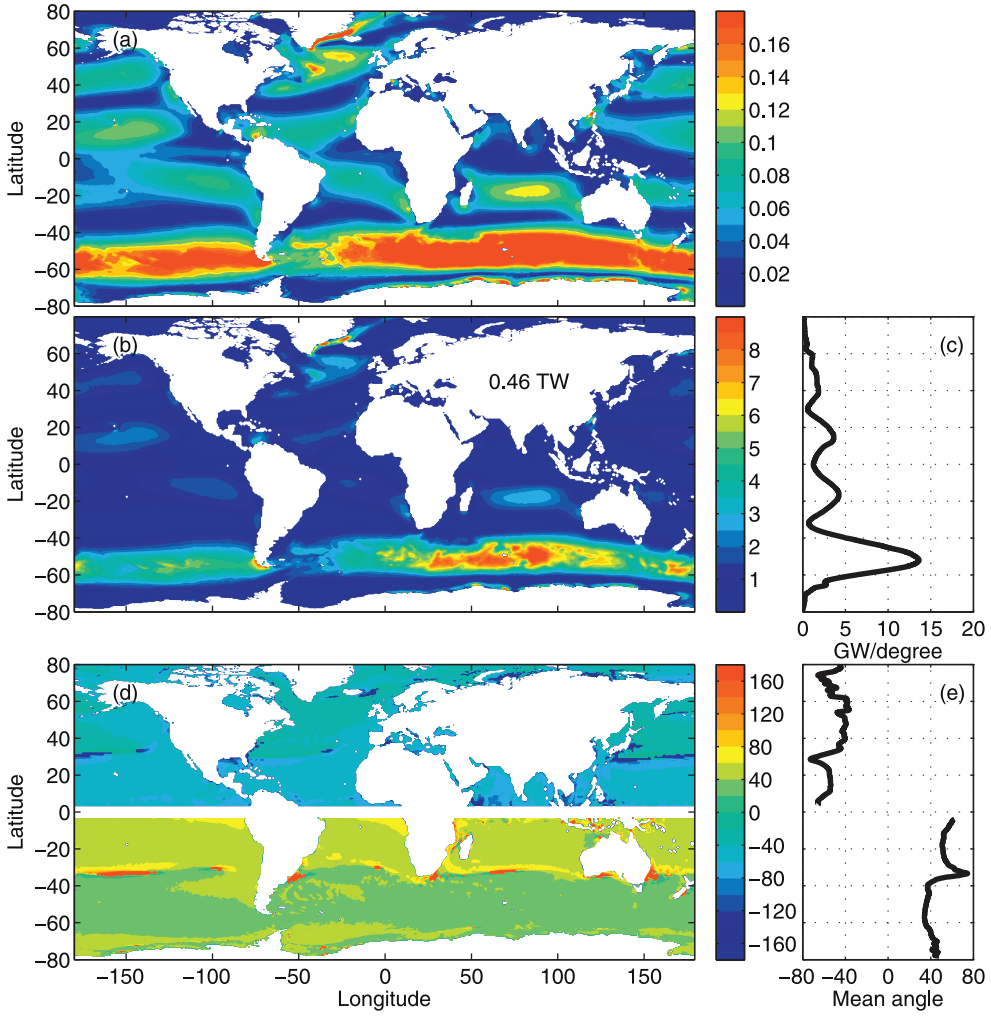

Fig. 5. (a) Seventeen-year average of wind stress (N/m^2) magnitude over the period 1999–2015. (b) The estimated $\overline{\tau}\cdot\overline{V_{ag}}$ (10^{-3} W/m^2) by applying the 17-year average wind stress to Eq. (11) and (c) the meridional distribution of the zonal integral of (b), (d) the angle (degrees, positive counterclockwise) between the 17-year average of wind stress and the surface ageostrophic currents and (e) the zonal mean angle (degrees).

Von Storch (2007) only allows their numerical model to represent 58% (77%) of the surface Ekman current. Second, Von Storch et al. (2007) forced their numerical model with daily wind stress. According to Section 4.4, this leads to an underestimate of 1.26 TW wind work due to the lack of the high frequency wind stress contribution (from daily to hourly) to the wind work on Ekman currents and not being able to resolve the near-inertial currents at latitudes poleward of 10°. Third, the reanalysis stores hourly surface output while Von Storch et al. (2007) stores snapshots every three days. This likely leads to an underestimate of the wind work in their study. For example, Von Storch et al. (2012) analyzed data from the German consortium project STORM/NCEP simulation, which was forced by 6-hourly NCEP-NCAR reanalysis-1 (Kalnay et al., 1996) wind stress, to estimate the wind work using accumulated second moments. They were able to obtain a 20% higher value in the eddy part of the wind work than the estimate in Von Storch et al. (2007) even with a thicker first layer of 10 m. As mentioned in Von Storch et al. (2012), the higher eddy part of wind work on surface currents in comparison with the estimate in Von Storch et al. (2007) can be a direct consequence of calculating the eddy part of wind work using accumulated second moments rather than snapshots sampled every three days.

5. Discussions and conclusions

In this study, we calculate the wind work on the surface currents from a 17-year global HYCOM reanalysis with hourly surface stress, surface currents, and SSH outputs. The reanalysis is forced with a wind stress formulation that takes into account the ocean surface currents. The hourly 10-m wind velocities are obtained from the 0.3125° resolution NCEP CFSR datasets. At every time step the surface stress is calculated using the CFSR 10-m wind velocities and surface currents from the reanalysis.

For the mean part of the wind work, our estimate of $\overline{\tau}\cdot\overline{V_g}$ agrees well with previous research (Wunsch, 1998; Hughes and Wilson, 2008) in both the global integral (0.81 TW) and the meridional variation of the zonal integral. However, the global integral of $\overline{\tau}\cdot\overline{V_{ag}}$ is estimated to be 1.28 TW, which is more than double the 0.54 TW estimate in Wang and Huang (2004). The reason for this significant difference is most likely due to the fact that there are large uncertainties in the estimate of the Ekman depth in Wang and Huang (2004). In addition, Wang and Huang (2004) used a constant angle of 45° between wind stress and surface Ekman currents in their estimate while this angle can have large spatial variations in the real ocean.

As for the eddy part of the wind work, the global integral of eddy wind work on the surface ageostrophic currents ($\overline{\tau'\cdot V'_{ag}}$) is 4.15 TW, much larger than the Wang and Huang (2004) 1.83 TW estimate. However, the fact that the global integral of $\overline{\tau'\cdot V'_g}$ is much smaller than $\overline{\tau}\cdot\overline{V_g}$ and the global integral of $\overline{\tau'\cdot V'_{ag}}$ is larger than that of $\overline{\tau}\cdot\overline{V_{ag}}$ agrees well with the previous studies by Wunsch (1998), Wang and Huang (2004), and Hughes and Wilson (2008).

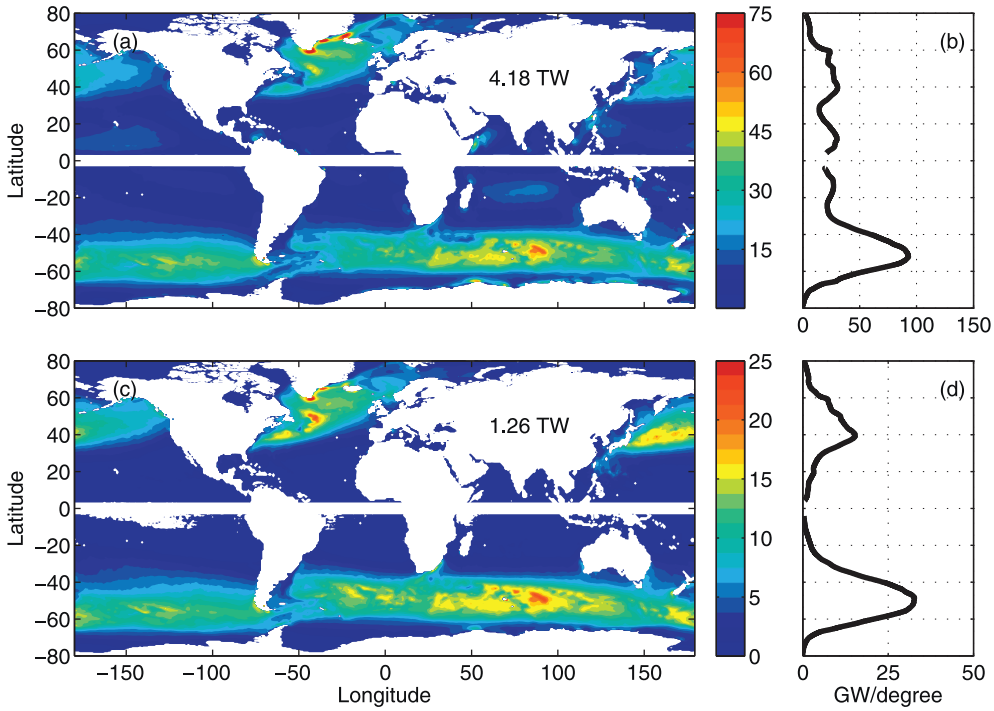

Fig. 6. Seventeen-year average (10^{-3} W/m^2) of (a) $\overline{\tau \cdot V_{ag}}$ over the period 1999–2015 calculated from daily average reanalysis outputs and (b) the corresponding meridional distribution of the zonal integral, (c) the difference of $\overline{\tau \cdot V_{ag}}$ between those calculated from hourly output (Fig. 4e) and daily average (Fig. 6a), and (d) the meridional distribution of the zonal integral of (c).

The spatial pattern of the wind work on the ageostrophic currents ($\overline{\tau \cdot V_{ag}}$) is very similar to that reported by Wang and Huang (2004, their Fig. 3) but the 5.44 TW global integral is much larger. The 3.14 TW difference can be attributed to three parts: 1) the wind work on the near-inertial currents contributes 0.5 TW, 2) the higher frequency wind stress (daily to hourly) contributes 0.86 TW wind work on surface Ekman currents, and 3) the remaining 1.78 TW difference most likely comes from the underestimation by Wang and Huang (2004) from overestimating the Ekman depth and using a constant 45° angle between the wind stress and surface Ekman currents rather than spatially varying angle as indicated by observations.

5.1. Sensitivity study of the different geostrophic average period to the wind work on ageostrophic currents

In this study, geostrophic currents are calculated from 10-day average reanalysis SSH fields and the ageostrophic currents are defined as the departure from the 10-day average geostrophic currents. The 10-day average period is an arbitrary choice chosen to be consistent with Wunsch (1998). Geostrophic flow also exists in periods less than 10 days and can contaminate the calculation of ageostrophic currents and thus the wind work on the ageostrophic currents. The difference is the eddy part of the high frequency wind work on the geostrophic currents. To address how sensitive is wind work on the ageostrophic currents to the choice of the geostrophic average period, we calculate the eddy part of wind work on geostrophic currents ($\overline{\tau' \cdot V'_{og}}$) using hourly and daily average reanalysis surface stress and SSH output to calculate geostrophic currents assuming geostrophic equilibrium.

$\overline{\tau' \cdot V'_{og}}$ calculated from hourly and daily average output shares very similar spatial patterns (not shown) with that from 10-day average output (Fig. 2). The global integral changes only by 0.008 and 0.015 TW (Table 5) when daily average and hourly reanalysis output are used to calculate wind work on geostrophic currents instead of the 10-day average. Those differences are negligible to the wind work on ageostrophic currents (5.44 TW). Thus, wind work on the ageostrophic currents is not sensitive to the choice of the geostrophic average period.

Table 5
Global integral (63°S - 63°N) of the eddy part of the wind work (TW) on geostrophic currents using different average periods. The equatorial region (within ± 3° from the equator) is omitted from the calculation.

Component	10-day average	Daily average	Hourly
$\overline{\tau'_x u'_g}$	−0.042	−0.037	−0.033
$\overline{\tau'_y v'_g}$	−0.057	−0.054	−0.051

5.2. Total wind work on the global ocean currents

The total wind work on the global ocean currents is estimated as 6.15 TW (Figure 3c and d) when calculated using hourly reanalysis output. The most important area is the ACC in the Southern Ocean (Fig. 3d), which contributes 46% to the total wind work. Another 20% comes from the tropical-subtropical region within ± 20° of the equator and 12% comes from Northern Hemisphere storm track regions in the area 40°−60°N. Previously, the total wind work on the global ocean currents was estimated to be 3.7 TW as the sum of the 0.88 TW input to the geostrophic currents (Wunsch, 1998), 2.3 TW input to the ageostrophic currents without near-inertial motion (Wang and Huang, 2004), and 0.5 TW input to the near-inertial currents (Alford, 2003). Our estimate, which contains all the spectrum mentioned above, is much larger. The equatorial region (within ± 3° of the equator) is omitted from our estimate and provides an additional 0.2 TW to the global integral of the total wind work to the global ocean circulation. The global integral in this study is integrated from 63°S - 63°N. Contributions beyond this region to the wind work on geostrophic currents and the mean part of wind work on the ageostrophic currents are negligible. But for the eddy part of wind work on the ageostrophic currents, there is an additional 0.4 TW poleward of 63°

5.3. Impact of the thickness of the surface layer

In Section 1.3, the classical Ekman spiral theory discussion indicates

that wind work on Ekman currents is reduced when calculated with vertical mean currents. In this section, we calculate wind work on the ageostrophic currents using the vertical mean ageostrophic currents in the top 5 m and 30 m to show how much of the wind work is reduced compared with the reanalysis results for June 2004. In these calculations, we assume the vertical shear of the geostrophic currents is negligible in the top 30 m of the water column to calculate the ageostrophic currents below the surface layer. The wind work on the ageostrophic currents calculated from the vertical mean ageostrophic currents in the top 5 m (30 m) is only 78% (15%) of that calculated using the currents in the top 1 m. In another words, the total wind work on the ageostrophic currents can be reduced by 22% (85%) when a 5 m (30 m) first layer thickness instead of 1 m is used in the reanalysis. Applying these ratios to the wind work on ageostrophic currents calculated with daily average output (4.18 TW, section 4.4) gives us 3.3 TW (0.6 TW) of wind work on ageostrophic currents if the HYCOM surface layer thickness is 5 m (30 m). These estimates are in closer agreement with 2.7 TW in Von Storch et al. (2007) who uses a first layer of 5 m thickness and the 0.3 TW in Huang et al., (2006) who uses a first layer of 30 m thickness.

5.4. Impact on the kinetic energy budget and dissipation in the Ekman layer

The estimate from this study is very useful for the global kinetic energy budget analysis since wind work on the surface currents is the most important mechanical energy source in maintaining the oceanic general circulation. Wind work on ageostrophic currents through the subinertial range is fully dissipated in the Ekman layer on supporting turbulence and mixing only in the steady state (Wang and Huang, 2004). The increase of wind work on the ageostrophic currents through the increase of the wind stress frequency clearly demonstrates that the high frequency variability can be important for inputting energy into the global ocean circulation. Since the majority of this additional energy must be dissipated inside the Ekman layer, this provides additional information of the mixing process inside the Ekman layer. How much of the wind work on the ageostrophic currents passes through the Ekman layer is unknown and is a topic for the future research. As suggested by Von Storch et al. (2007), about 5% (0.14 TW) of the wind work on ageostrophic currents escapes the surface layer of 110 m thickness. The 110 m depth is much deeper than the Ekman depth in general. But even if we apply the same ratio to the reanalysis, 0.3 TW of wind work on the ageostrophic currents would be transported into the sub-surface layer and play a major role in the oceanic circulation.

Acknowledgements

The authors thank the editor and the anonymous reviewers for their input to improve the original manuscript. Z. Yu was supported by the Karle's Research Fellowship through the Naval Research Laboratory. Y. Fan was funded by the “6.1 The Effect of Langmuir Turbulence in Upper Ocean Mixing” project sponsored by the Office of Naval Research. E. J. Metzger was funded by the “6.1 Kuroshio and Ryukyu Current Dynamics” project sponsored by the Office of Naval Research under program element 0601135 N. O. M. Smedstad is supported through a contract with Vencore. Computer time was provided by the Department of Defense (DoD) High Performance Computing Modernization Program and the simulations were performed on the Cray XC40 (Conrad) at the Navy DoD Supercomputing Resources Center, Stennis Space Center, MS. This is NRL contribution NRL/JA/7320-17-3473. It has been approved for public release and distribution is unlimited.

References

Alford, M.H., 2001. Internal swell generation: the spatial distribution of energy flux from the wind to mixed-layer near-inertial motions. J. Phys. Oceanogr. 31, 2359–2368.
Alford, M.H., 2003. Improved global maps and 54-year history of wind-work on ocean inertial motions. Geophys. Res. Lett. 30. https://doi.org/10.1029/2002GL016614.
Bleck, R., 2002. An oceanic general circulation model framed in hybrid isopycnic-Cartesian coordinate. Ocean Model. 4, 55–88.
Chereskin, T.K., 1995. Direct evidence for an Ekman balance in the California Current. J. Geophys. Res. 100, 18261–18269.
Cummings, J.A., 2005. Operational multivariate ocean data assimilation. Q. J. R. Meteorol. Soc. 131, 3583–3604.
Cummings, J.A., Smedstad, O.M., 2013. Variational data assimilation for the global ocean. In: Park, S.K., Xu, L. (Eds.), Data Assimilation for Atmospheric, Oceanic, and Hydrologic Applications II Springer-Verlag, Berlin Heidelberg. http://dx.doi.org/10.1007/978-3-642-35088-7_13.
Cushman-Roisin, B., 1994. Introduction to Geophysical Fluid Dynamics. Prentice Hall, pp. 320.
D'Asaro, E.A., 1985. The energy flux from the wind to near-inertial motions in the surface mixed layer. J. Phys. Oceanogr. 15, 1043–1059.
Duhaut, T.H.A., Straub, D.N., 2006. Wind stress dependence on ocean surface velocity: implications for mechanical energy input to ocean circulation. J. Phys. Oceanogr. 36, 202–211.
Fofonoff, N.P., 1981. The gulf stream system. evolution of physical oceanography. In: Warren, B.A., Wunsch, C. (Eds.), Scientific Surveys in Honor of Henry Stommel. The MIT Press, pp. 112–139.
Helber, R.W., Townsend, T.L., Barron, C.N., Dastugue, J.M., Carnes, M.R., 2013. NRL memorandum report NRL/MR/7320–13-9364. http://www7320.nrlssc.navy.mil/pubs/2013/helber1-2013.pdf.
Huang, R.X., Wang, W., Liu, L.L., 2006. Decadal variability of wind-energy input to the world ocean. Deep Sea Res. II 53, 31–41. https://doi.org/10.1016/j.dsr2.2005.11.001.
Hughes, C.W., Wilson, C., 2008. Wind work on the geostrophic ocean circulation: an observational study on the effect of small scales in the wind stress. J. Geophys. Res. 113. https://doi.org/10.1029/2007JC004371.
Kalnay, E., 1996. Ocean circulation and tropical variability in the coupled ECHAM5/MPI-OM. J. Climate 19, 3952–3972.
Kelly, K.A., Dickinson, S., McPhaden, M.J., Johnson, G.C., 2001. Ocean currents evident in satellite wind data. Geophys. Res. Lett. 28, 2469–2472.
Lenn, Y.-D., Chereskin, T.K., 2009. Observations of Ekman currents in the Southern Ocean. J. Phys. Oceanogr. 39, 768–779. https://doi.org/10.1175/2008JPO3943.1.
Luo, J.-J., Masson, S., Roeckner, R., Madec, G., Yamagata, T., 2005. Reducing climatology bias in an ocean-atmosphere CGCM with improved coupling physics. J. Climate 18, 2344–2360.
McWilliams, J., Huckle, E., Liang, J-H, Sullivan, P., 2012. The wavy Ekman layer: Langmuir circulations, breaking waves, and Reynolds stress. J. Phys. Oceanogr. 42, 1793–1816. https://doi.org/10.1175/JPO-D-12-07.1.
McWilliams, J., Sullivan, P., Moeng, C., 1997. Langmuir turbulence in the ocean. J. Fluid Mech. 334, 1–30.
Metzger, E.J., Smedstad, O.M., Thoppil, P.G., Hurlburt, H.E., Cummings, J.A., Wallcraft, A.J., Zamudio, L., Franklin, D.S., Posey, P.G., Phelps, M.W., Hogan, P.J., Bub, F.L., Dehaan, C.J., 2014. US Navy Operational Global Ocean and Arctic ice prediction systems. Oceanography 27, 32–43.
Munk, W., Wunsch, C., 1998. Abyssal recipes II: energetics of tidal and wind mixing. Deep Sea Res. I 45, 1977–2010.
Oort, A.H., Anderson, L.A., Peixoto, J.P., 1994. Estimates of the energy cycle of the oceans. J. Geophys. Res. 99, 7665–7688.
Pacanowski, R.C., 1987. Effect of equatorial currents on surface stress. J. Phys. Oceanogr. 17, 833–838.
Price, J.F., Weller, R.A., Schudlich, R.R., 1987. Wind-driven ocean currents and Ekman transport. Science 238, 1534–1538.
Saha, S., 2010. The NCEP climate forecast system reanalysis. Bull. Amer. Meteor. Soc. 91, 1015–1057. http://dx.doi.org/10.1175/2010BAMS3001.1.
Scott, R.B., Xu, Y., 2009. An update on the wind power input to the surface geostrophic flow of the world ocean. Deep Sea Res. 56. https://doi.org/10.1016/j.dsr.2008.09.010.
Thoppil, P., Metzger, E.J., Hurlburt, H.E., Smedstad, O.M., Ichikawa, H., 2015. The current system east of the Ryukyu Islands as revealed by a global ocean reanalysis. Prog. Oceanogr. 141, 239–258. https://doi.org/10.1016/j.pocean.2015.12.013.
Von Storch, J.S., Sasaki, H., Marotzke, J., 2007. Wind-generated power input to the deep ocean: an estimate using a 1/10° general circulation model. J. Phys. Oceanogr. 37. https://doi.org/10.1175/JPO3001.1.
Von Storch, J.S., Eden, C., Fast, I., Haak, H., Hernandez-Deckers, D., Maier-Reimer, E., Marotzke, J., Stammer, D., 2012. An estimate of the Lorenz energy cycle for the world ocean based on 1/10° STORM/NCEP simulation. J. Phys. Oceanogr. 42. https://doi.org/10.1175/JPO-D-12-079.1.
Wang, W., Huang, R.X., 2004. Wind energy input to the Ekman layer. J. Phys. Oceanogr. 34, 1267–1275.
Watanabe, M., Hibiya, T., 2002. Global estimates of the wind-induced energy flux to inertial motions in the surface mixed layer. Geophys. Res. Let. 29. https://doi.org/10.1029/2001GL014422.
Wunsch, C., 1998. The work done by the wind on the oceanic general circulation. J. Phys. Oceanogr. 28, 2332–2340.
Xu, Y., Scott, R.B., 2008. Subtleties in forcing eddy resolving ocean models with satellite wind data. Ocean Model. 20, 240–251. https://doi.org/10.1016/j.ocemod.2007.09.003.
Yu, Z., Metzger, E.J., Thoppil, P., Hurlburt, H.E., Zamudio, L., Smedstad, O.M., Na, H., Nakamura, H., Park, J.-H., 2015. Seasonal cycle of volume transport through Kerama gap revealed by a 20-year global hybrid coordinate ocean model reanalysis. Ocean Model. 96, 203–213. https://doi.org/10.1016/j.ocemod.2015.10.012.
Yu, Z., Metzger, E.J., Fan, Y., 2017. The impact of ocean surface currents on Sverdrup transport in the midlatitude north Pacific via the wind stress formulation. J. Phys. Oceanogr. 47. https://doi.org/10.1175/JPO-D-16-0155.1.
Zhai, X., Johnson, H.L., Marshall, D.P., Wunsch, C., 2012. On the wind power input to the ocean general circulation. J. Phys. Oceanogr. 42. https://doi.org/10.1175/JPO-D-12-09.1.